NASA TECHNICAL MEMORANDUM

NASA TM X-74024

NASA TM X-74024

EVALUATION OF COMMERCIAL PYROELECTRIC DETECTORS

by James B. Robertson and Roger K. Crouch

April 197?

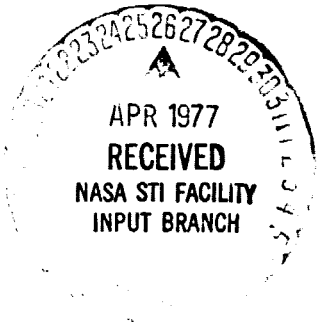

National Aeronautics and Space Administration

Langley Research Center
Hampton, Virginia 23665

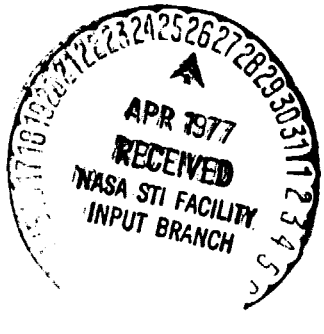

1. Report No.	2. Government Accession No.	3. Recipient's Catalog No.
NASA TM X-74024		

4. Title and Subtitle	5. Report Date
Evaluation of Commercial Pyroelectric Detectors	April 1977
	6. Performing Organization Code

7. Author(s)	8. Performing Organization Report No.
James B. Robertson, Roger K. Crouch	
	10. Work Unit No.
9. Performing Organization Name and Address	
NASA Langley Research Center Hampton, VA 23665	11. Contract or Grant No.
	13. Type of Report and Period Covered
12. Sponsoring Agency Name and Address	Technical Memorandum
National Aeronautics & Space Administration Washington, DC 20546	14. Sponsoring Agency Code

15. Supplementary Notes

16. Abstract

Currently available pyroelectric detectors are capable of room temperature operation and have detectivities of 4×10^8 cm $Hz^{1/2}/w$ and spectral sensitivities from the visible to greater than 100 um. Because pyroelectrics are thermal detectors, their spectral response can be made nearly flat over broad spectral regions by the use of appropriate black surface coating.

A series of commercially available pyroelectric detectors made from PVF_2, LTO, SBN, and TGS have been evaluated in terms of responsivity and detectivity (D*) as a function of frequency. It was found that the performance of the detectors evaluated was very different, depending upon the manufacturer of the detector, and this dependency was primarily related to the thickness of the various detectors. The best detectors of each material were comparable in performance at frequencies around 10 Hz but differed radically at frequencies above 100 Hz.

17. Key Words (Suggested by Author(s))	18. Distribution Statement
IR Detectors, Pyroelectric Strontium barium niobate Lithium tantalate	Unclassified - Unlimited

19. Security Classif. (of this report)	20. Security Classif. (of this page)	21. No. of Pages	22. Price*
Unclassified	Unclassified	15	$3.50

*For sale by the National Technical Information Service, Springfield, Virginia 22161

SUMMARY

Currently available pyroelectric detectors are capable of room temperature operation and have detectivities of 4×10^8 cm Hz $^{1/2}$/w and spectral sensitivities from the visible to greater than 100 μm. Because pyroelectrics are thermal detectors, their spectral response can be made nearly flat over broad spectral regions by the use of appropriate black surface coatings.

A series of commercially available pyroelectric detectors made from PVF_2, LTO, SBN, and TGS have been evaluated in terms of responsivity and detectivity (D^*) as a function of frequency. It was found that the performance of the detectors evaluated was very different, depending upon the manufacturer of the detector, and this dependency was primarily related to the thickness of the various detectors. The best detectors of each material were comparable in performance at frequencies around 10 Hz but differed radically at frequencies above 100 Hz.

INTRODUCTION

Currently available pyroelectric detectors are capable of room temperature operation and have detectivities of 4×10^8 cm Hz/w and spectral sensitivities from the visible to greater than 100 μm. Because pyroelectrics are thermal detectors, their spectral response can be made nearly flat over broad spectral regions by the use of appropriate black surface coatings.

NASA's commitment to air pollution monitoring and thermal mapping of the earth requires photodetection in the 3 μm to 20 μm spectral region. If pyroelectric detectors can be used in these applications in place of cooled photoconductive and photovoltaic detectors, a large savings in volume, weight, and power can be realized.

The purpose of this report is to give to potential users of pyroelectric detectors a brief introduction to the operation and characteristics of pyroelectric detectors and to present performance data on pyroelectric detectors which are currently available on the market. All of the detectors evaluated for this report were purchased prior to March 1976.

TECHNICAL BACKGROUND

A pyroelectric detector is a thermal-to-electrical transducer. By absorbing incident light and converting it to heat, the pyroelectric detector becomes an optical-to-electrical transducer.

Pyroelectric materials are insulators with a spontaneous polarization that changes with temperature. A detector is made from the material by cutting the material into wafers with the plane of the wafer normal to the polar axis and making electrical contact to the flat sides. The detector is essentially a capacitor with the pyroelectric material between the plates.

Radiation incident upon the detector is absorbed by the detector causing an increase in temperature. The change in temperature causes a change in the polarization of the pyroelectric material and, thereby, a change in the amount of charge attracted to its surface. The magnitude of the change of polarization per unit change of temperature is called the pyroelectric coefficient, p. If the incident radiation is chopped, the detector becomes an AC generator, and the charge flowing to and from the surface via an external circuit can be measured.

The impedance of the pyroelectric detectors at normal operating frequencies is very high ($\sim 10^{13}$ ohm), and for practical applications, a field effect transistor (FET) must be used to lower the impedance. Typical circuits are shown

in figure 1. Since practical use of the pyroelectric requires the FET, meaningful performance data must include the performance of the FET. For the remainder of this paper, the word "detector" shall refer to the pyroelectric chip and any integrated impedance-converting circuit. The pyroelectric chip with its two surface contacts will be referred to as "detector element."

There are many pyroelectric materials from which detectors may be made. Only four of these, however, have survived the competition and made it to the marketplace. These are:

(1) Triglycine sulfate (TGS) --- Triglycine sulfate was the material used in the first marketed detector. It is difficult to handle and is hygroscopic, but produces detectors with the highest detectivity.

If the triglycine sulfate is made with deuterium atoms in place of the hydrogen atoms, the resulting material, called deuterated triglycine sulfate (DTGS), has the advantage of a higher Curie temperature than TGS.

(2) Lithium tantalate, (LTO) --- Lithium tantalate is inexpensive, easy to handle, nonhygroscopic, but not as sensitive as TGS.

(3) Strontium barium niobate (SBN) --- Strontium barium niobate is nonhygroscopic and is more difficult to process than LTO; detectivity values just below TGS are possible.

(4) Polyvinylidene fluoride (PVF_2) --- Polyvinylidene fluoride is flexible plastic film, nonhygroscopic. It is not competitive for small area detectors, but is the best available material for large area (~1 cm dia.) detectors.

EXPERIMENTAL

Detectors from nine different manufacturers were evaluated. The detectors with their pertinent design information are listed in Table 1. FET impedance-converter circuits were added to all detectors not so supplied by the manufacturer. All detectors except the PVF_2 were operated in the voltage mode (fig. 1a). The PFV_2 detector was operated in the current mode (fig. 1b) being supplied this way with the circuit within the detector housing.

The signal voltage and noise voltage of each detector was measured as a function of chopping frequency over the frequency range of 2 Hz to 500 Hz. From these data, responsivities (R) and detectivities (D^*) were calculated.

Equipment.- A schematic of the experimental setup is shown in figure 2.

The radiation source was a 500° K, conical cavity, black-body. Temperature of the black body was monitored with a thermocouple which was connected to an ice-point reference. The radiation was chopped with a 23 cm diameter wheel. Typical source aperture was 0.300 cm^2; typical source-to-detector distance was 15 cm; and typical chopper form factor (ref. 1) was 0.422, giving a typical flux density of 6.3×10^{-5} watt/cm^2.

Signals from the detector were amplified by a Quan Tech 206C preamp and measured with a Quan Tech 304A wave analyzer set to a 1 Hz bandwidth.

Detector noise was measured with the Quan Tech 304A set to 1 Hz bandwidth and a 100 second integration time. The chopper motor was stopped, and the radiation was blocked during the noise measurements.

The equations used are listed below.

$$H = \frac{ff \times \sigma \times T^4 \times A_s}{\pi d^2}$$

$$R = \frac{S}{HA_d}$$

$$D^* = \frac{S/N\ \sqrt{\Delta f}}{H\ \sqrt{A_d}}$$

where:

H = irradiance, watt cm^{-2}

ff = chopper form factor (ref. 1)

σ = Stefan-Boltzmann Constant, 5.67×10^{-12} W cm^{-2} $^{\circ}K^{-4}$

T = black-body temperature, $^{\circ}K$

A_s = source aperture, cm^2

d = source-to-detector distance, cm

R = responsivity, volt/watt

S = signal voltage, volt

A_d = active area of detector, cm^2

D^* = detectivity, cm $Hz^{1/2}$ $watt^{-1}$

N = noise voltage, volt

Δf = amplifier bandwidth, Hz

RESULTS

Figure 3 is a plot of D^* versus frequency of one each of the nine different brands of detectors. Where more than one detector from a given manufacturer was tested, a curve representative of the mean performance was chosen. Figure 3a presents curves of the best performing detectors of each material; LTO, DTGS, PVF_2, and SBN. It should be noted that the PVF_2 was operated with a built-in operational amplifier in the current mode.

Figure 3b presents D^* versus frequency of all of the LTO detectors. The curves in 3a and 3b are the same as in figure 3; they are shown separately to aid in comparison. Figure 4 presents the noise voltage versus frequency of one detector of each material.

DISCUSSION

On figure 3 several observations can be made: the performance of all detectors peak at 20 Hz or below. D^* values are within one order of magnitude at 10 Hz and spread to 2.5 orders of magnitude at 500 Hz. There is a larger difference between different manufacturers using the same material (LTO) than between detectors of different material.

In figure 3b, the large differences in performance of different models of LTO detectors can be seen. The active areas of the detector chips range from 0.00785 cm^2 to 0.0314 cm^2 but show no correlation with performance. Three of the detectors have windows and two do not, but no effect is noticed here. The use of windows decreases the responsivity of the detector by reducing the amount of energy reaching the detector chip, however the windows decrease noise by reducing airborne acoustics, by reducing thermal fluctuations due to air currents, and protecting by the detector from moisture and dirt.

The differences in performance are taken to be due to wafer thickness, wafer mounting, and choice of FET's; with thickness being the primary factor. The thicknesses of the lithium tantalate chips of figure 3b are:
#5 - 12.5 μm, #3 - 8.5 μm, #2 - 20 μm, #4 - 25 μm, #1 - 70 μm.

The noise voltage versus frequency curves for one detector of each material are shown in figure 4. Again, it must be noted that the PVF_2 detector is operated in the current mode. The noise of the PVF_2 detector is dominated by the noise contribution from the amplifier current noise. The curve should not be used to compare PVF_2 to other materials but is given as an example of noise from a current-mode-operated detector.

REFERENCES

1. Hudson, R. D., Jr.: Infrared System Engineering. John Wiley and Sons, 1969, pp. 323 -327.

TABLE 1

ID No.	Manufacturer	Model No.	Detector area (cm^2)	Detector thickness (μm)	Window Material
PVF_2	A. D. Little	B100/off	.785	10	KRS-5
DTGS	Barnes Engineering	T-300	.20	10	KRS-5
SBN#1	Harshaw Chemical	PV3	.04	250	None
SBN#2	Honeywell	LK191	.0026	20	Ge (coated)
LTO#1	Eltec	404	.0314	70	Ge
LTO#2	Laser Presision	kT-2210	.00784	20	IR-II
LTO#3	Martin-Marietta	Laboratory device	.01	8.5	None
LTO#4	Molectron	P1-71	.00785	25	None
LTO#5	Servo	1401	.01	12.5	KRS-5

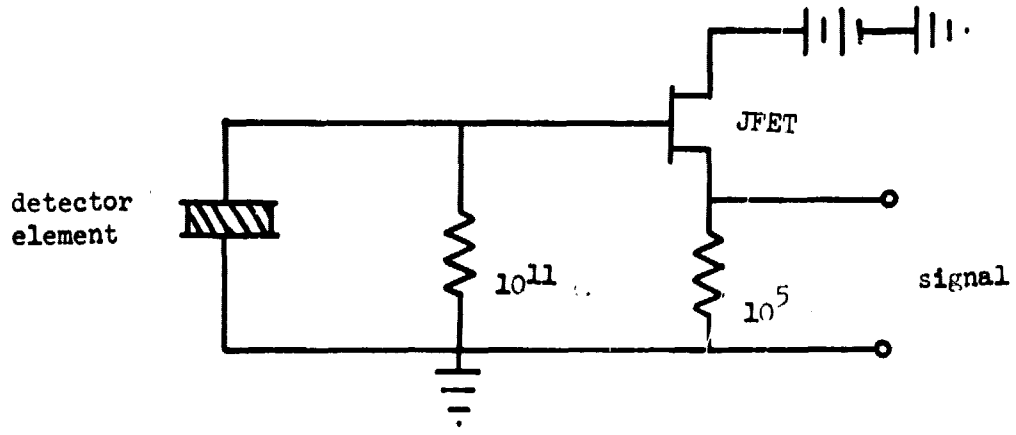

(a) Voltage mode

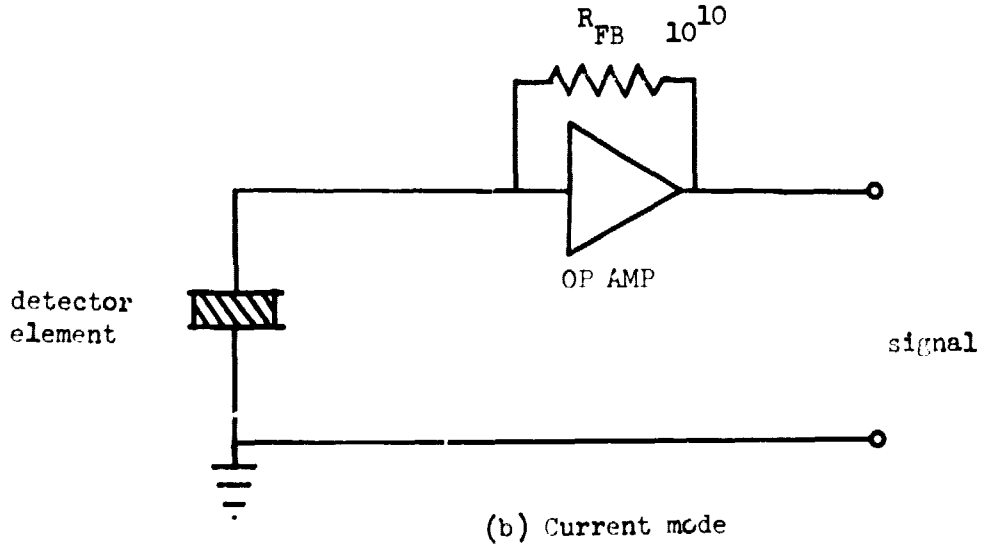

(b) Current mode

Figure 1. Detector circuits used for determination of D^*

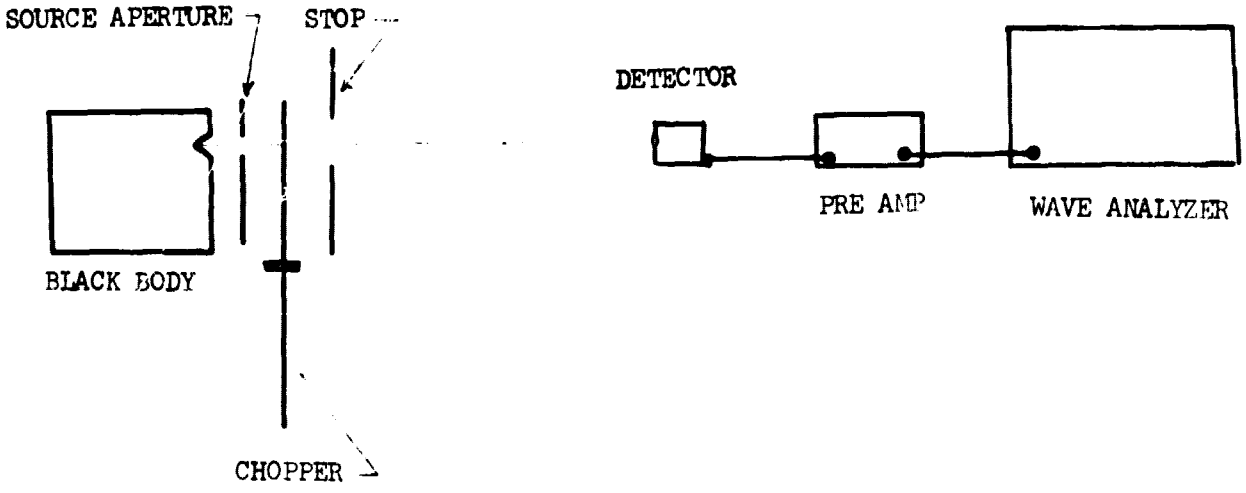

Figure 2. Experimental setup for evaluation of detectors

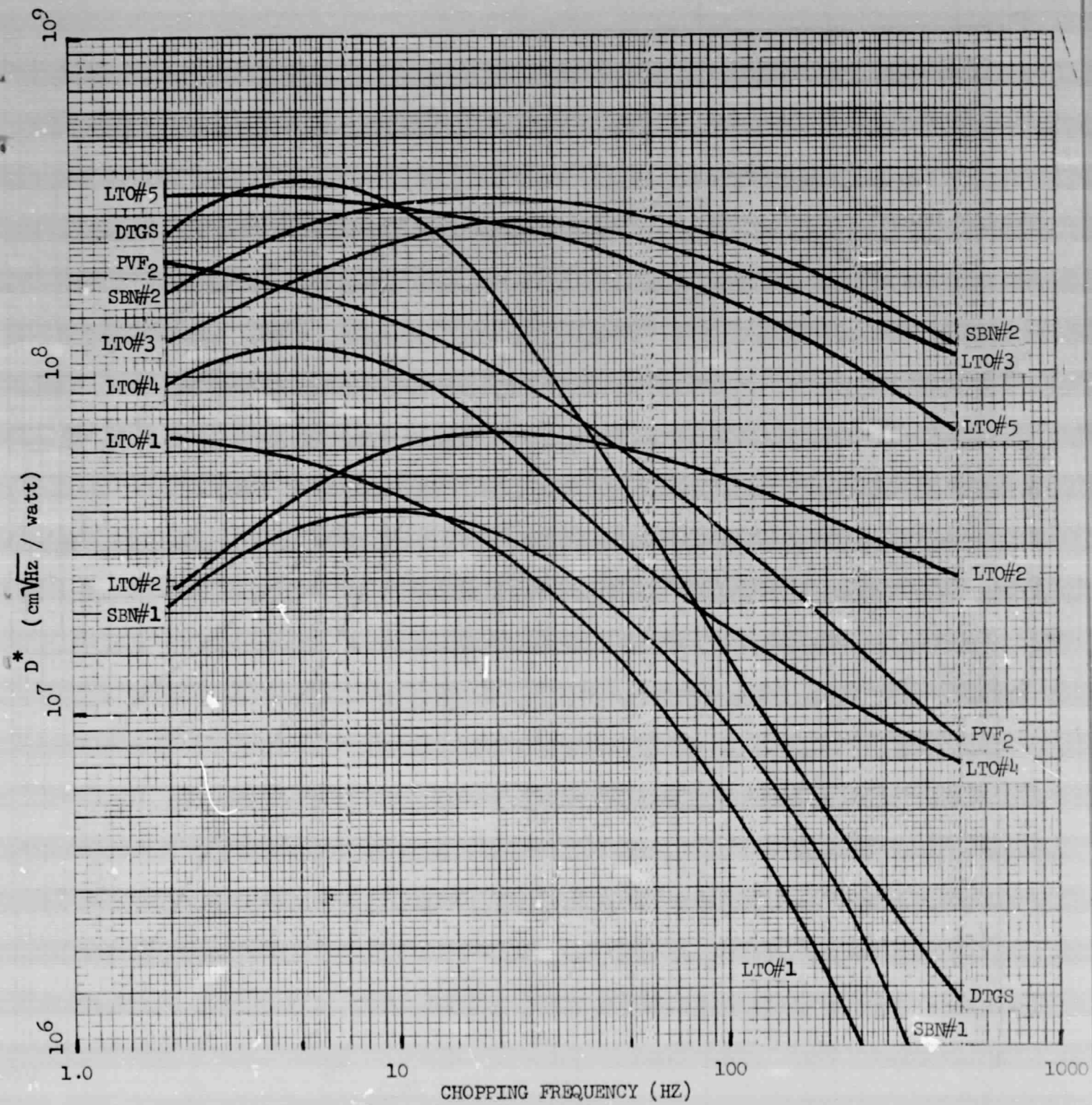

Figure 3. Performance curves of one detector of each manufacturer.

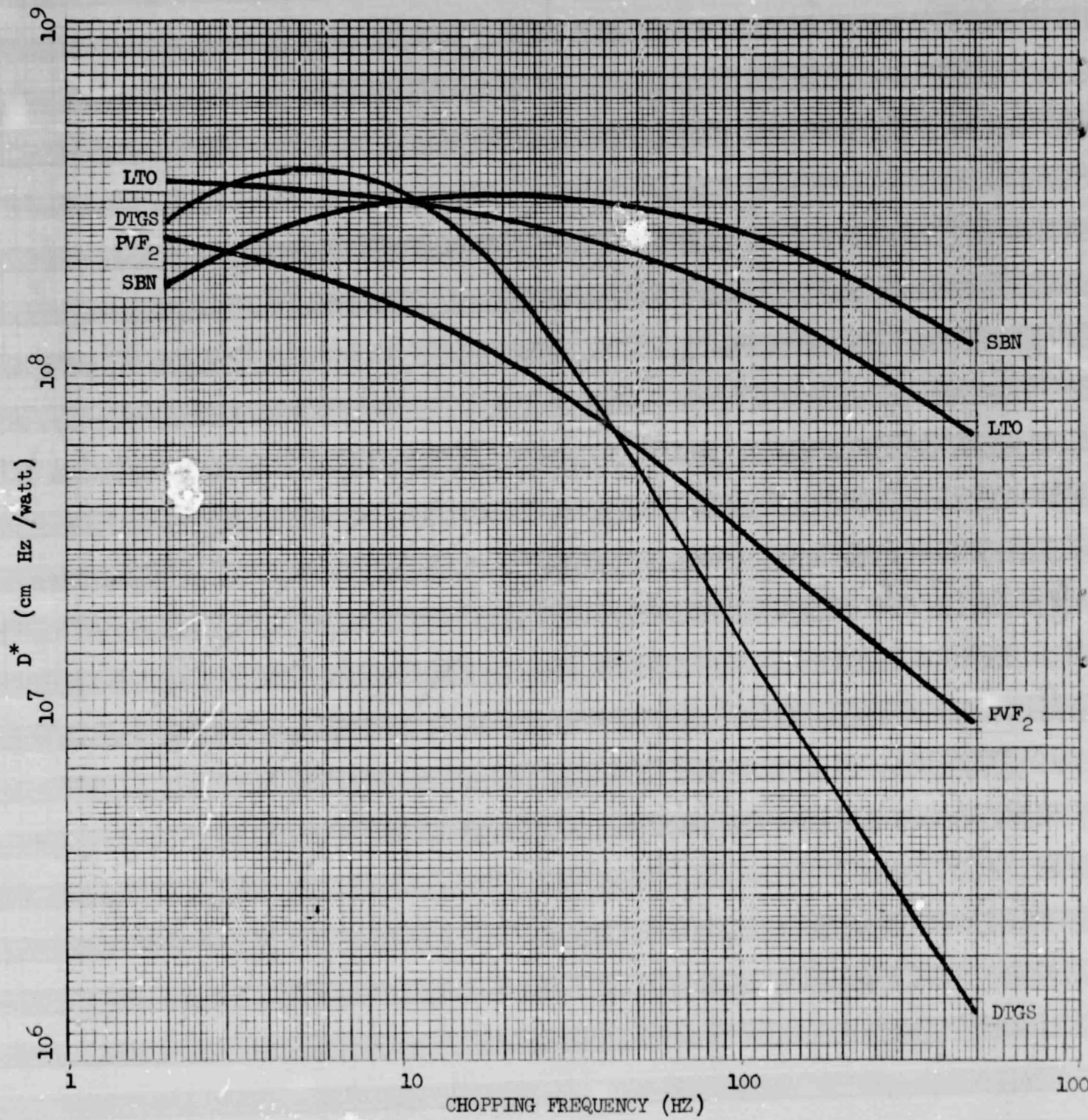

Figure 3a. Performance curves of the best detectors of each material.

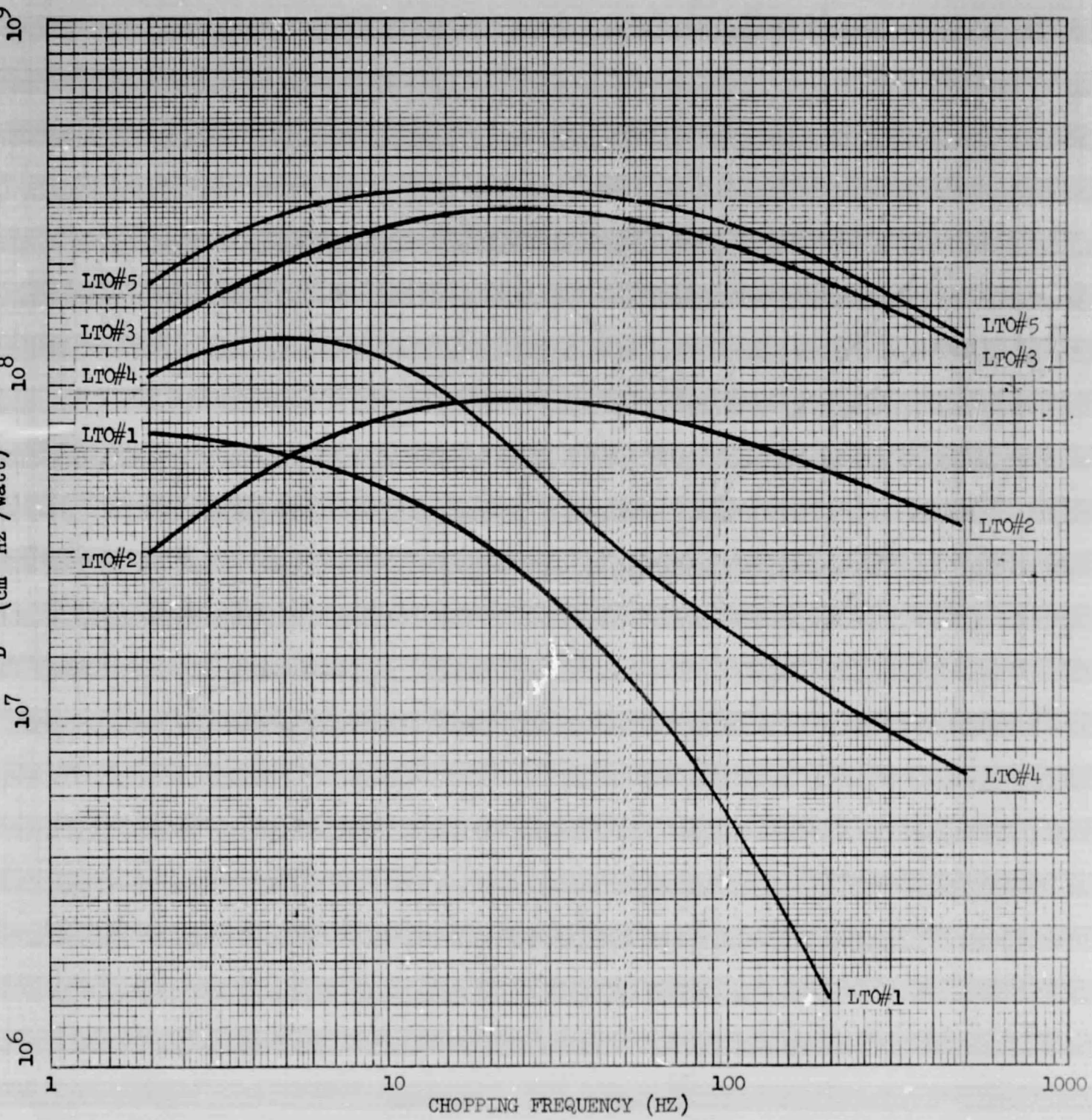

Figure 3b. Performance curves, one of each lithium tantalate manufacturer

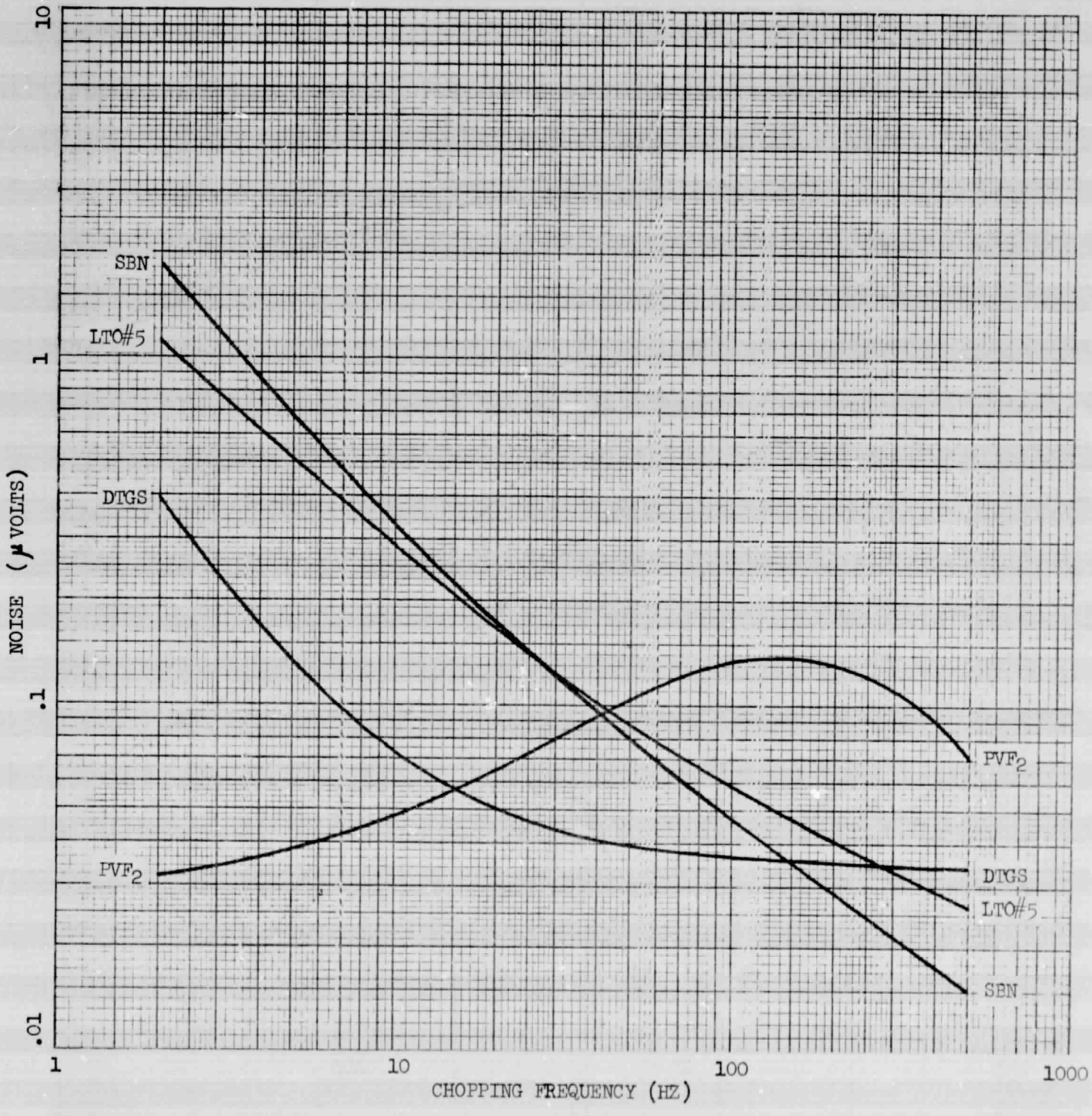

Figure 4. Noise curves, one of each material